Humidity Effects on Unsteady Characteristics of Supersonic Flow

Mem. Muroran Inst. Tech., 64(2014) 61~68

特　　集

Humidity Effects on Unsteady Characteristics of Supersonic Flow

Shohei TAKAGI [*1], Takuya UEMURA [*2] Yutaka HIRATA [*2] and Kosuke TAKADA [*2]

(Received 28th November 2014, Accepted 22nd January 2015)

Abstract

In supersonic wind tunnels, the humidity content of the working fluid is known to have a significant effect on flow conditions in the test section. The intent of this paper is to evaluate the influence of moisture on the test section flow quality for the indraft supersonic wind tunnel located at the Muroran Institute of Technology. The static-pressure fluctuation is measured by means of an unsteady pressure sensor buried in a 10-degree-aperture cone model installed in the test section. The results show that supersonic flow at Mach 2 is contaminated by the self-sustained oscillation of a condensation shock wave for ambient relative humidity greater than approximately 50%. It is also found that for the Mach 2 flow, that the ratio of the static-pressure fluctuation to the dynamic pressure is less than 0.1%, if the absolute humidity is kept below a critical value of 2[g/m^3]. Experimental observations also reveal that the three-dimensional boundary-layer transition process is hypersensitive to the influence of free-stream humidity.

Keywords: Supersonic flow, humidity, condensation shock wave, free-stream property

1 INTRODUCTION

Dry air is generally used in supersonic ground test facilities, in order to avoid the condensation of water particles present in humid air. When humid air is expanded to supersonic conditions, a supersaturated condition often results, wherein no condensation occurs even when flow temperatures drop below the dew point. However, the generation of tiny water droplets in the flow for any reason, spawns a sudden, homogenous condensation process. When water particles are condensed in a supersonic nozzle, latent heat is also released. A condensation shock wave forms downstream of the nozzle throat, and due to the large latent-heat release, thermal choking results in the self-sustained oscillation of the shock wave. The mechanism for this oscillation has been reasonably explained in a series of experimental studies by Matsuo[1, 2] et.al., using a Ludwieg tube. The latent-heat release also influences the accuracy of a Pitot-static tube for Mach number measurements[3-5]. Numerical calculations[6] for viscous flow at large subsonic Mach number, have shown that the lift-to-drag ratio is decreased as relative humidity is increased, due to the presence of this condensation shock wave.

*1 Muroran Institute of Technology, Aerospace Plane Research Center

*2 Muroran Institute of Technology, Division of Aero- space Engineering (Completed)

Since the supersonic wind tunnel located at the Muroran Institute of Technology (MIT henceforth) is of the indraft type, the supersonic flow in the test section is expected to be much quieter than that attained in equivalent blowdown-type wind tunnels, which employ a high pressure reservoir tank, with the attendant flow noise created when the flow exits this tank and enters the duct upstream of the test section. However, because ambient atmospheric humidity can produce additional disturbances as discussed above, it is important that the flow quality of any such indraft tunnel be assessed and quantified, especially for potential use in the study of laminar-to-turbulent transition, which is well known to be sensitive to free-stream noise.

The objective of the present paper is to evaluate the flow quality of the MIT wind tunnel, taking into account the influence of atmospheric conditions such as temperature, pressure, humidity and so forth. In order to evaluate the flow quality in the test section, static-pressure fluctuations in combination with condensation density are measured. A 10-degree-aperture cone (known to be the canonical model for static-pressure fluctuation measurements) was newly prepared for the present research and installed in the middle of the test section with an unsteady pressure sensor buried within the model. Further since light is scattered by tiny water droplets in the mist created by condensation, a sophisticated new method, which employs five sets of laser-photo diodes aligned to the axial flow, was invented to evaluate the condensation density in the test section. It is well-known that boundary-layer transition

is sensitive to the disturbance environment in the mean flow, and the flow quality is often judged by the observed absence or presence of certain disturbance modes. For example, three-dimensional boundary layers exhibit instabilities to both stationary and traveling disturbance modes. Since both modes are sensitive to flow disturbances[7-9], the appearance of these modes is often used as an indicator of the flow quality. Low free-stream disturbances favor the stationary mode and vice versa. It is well-known that stationary mode is hypersensitive to surface roughness. Thus, surface-flow visualization by means of surface-oil flow technique on a yawed circular cylinder model (which typifies swept-wing flow near the leading edge) is often made to confirm the low free-stream disturbance environment. In addition, hot-wire measurement is made to observe the traveling mode.

2 Experimental apparatus

2.1 Supersonic wind tunnel

For Mach 2, 3 and 4 flows, the MIT supersonic wind tunnel has three different nozzle blocks which are 2m in streamwise length and expand vertically while the transverse dimension is held constant, resulting in a 400 mm square test section. Two Schlieren windows are installed on the side walls of the test section and the Mach 2 nozzle block was used for the present experiment. The tunnel outlines are illustrated in Fig.1.

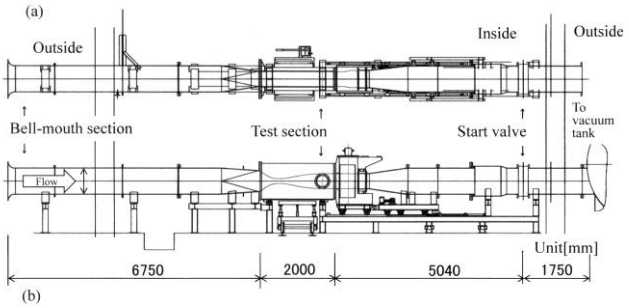

Fig. 1 MIT supersonic wind tunnel. (a) Plan view and (b) Side view.

Atmospheric air is sucked through a round-shaped bell mouth installed outdoors, and a conversion duct installed between the bell mouth and the nozzle block with a diameter of about 1m changes the round cross section to a rectangular shape. Downstream of the nozzle block, a sting holder for model support is mounted in the test section, and aft of the sting, a butterfly valve for intermittent operation is installed. Further downstream of the valve, five vacuum tanks with a total volume of 500 cubic meters are installed, allowing a blow duration of roughly 12 seconds independent of nozzle block. More details regarding this wind tunnel except for the tanks can be also seen in Ref. 10.

2.2 Condensation-density measurement and absolute humidity

When atmospheric humidity is high, the supersonic flow in the test section is perceptibly clouded due to condensation. Since this condensate consists of tiny ice particles that scatter light, the condensation density can be evaluated using a laser beam across the main flow in combination with a photo diode receiving the permeated laser beam. For the present experiment, inexpensive red-color laser pointers with a wavelength of 650 [nm] and a PIN photo diode with maximum sensitivity at 970[nm] (Hamamatsu Photonix Model S6775) were employed. Although this photo diode does not have its maximum sensitivity at the wavelength of the laser beam, it was found that the beam receiver has sufficient sensitivity to evaluate the condensation density.

Because high humidity air lends to self-sustained oscillation in the supersonic nozzle, both time-averaged as well as time-dependent components of photo-diode output were observed. Furthermore, oscillating patterns in the streamwise direction were tracked, thus providing a measure of convective velocity from the phase delay between time traces. To accomplish this, five identical sets of the laser-photo diodes separated by a streamwise distance of 45[mm] were horizontally installed in the streamwise direction as shown in Fig.2 and these outputs are simultaneously acquired at a sampling rate of 5[μs] or 10[μs] with the use of an NF Block Model EZ-7510, which will be mentioned in detail in subsection 2.4.

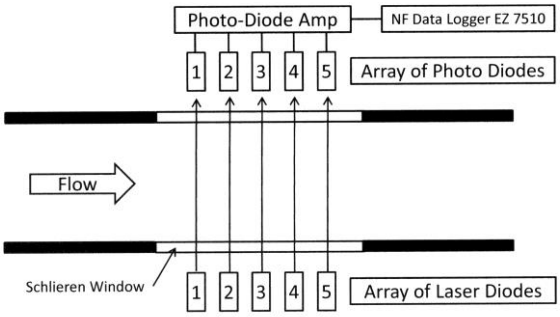

Fig. 2 Five pairs of laser-photo diodes horizontally aligned in streamwise direction with an interval of 45[mm] in test section downstream of supersonic nozzle.

The absolute humidity D[g/m^3] of the atmospheric air was calculated from the relative humidity U[%] with the use of the following psychrometric relations (see Ref. 11):

$$D = U \times 0.794 \times \mathrm{EXP}(e)/100, \quad (1)$$

$$e = (6096.9385/T + 21.2409642 - 0.02711193 \times T + 1.673952 \times 10^{-5} \times T^2 + 2.4335 \times \ln(T))/(1 + 0.00366 \times t),$$

where e is the evaporated pressure[Pa], T at absolute temperature [K] is T=273.15+t, t being the dry air temperature in [$^\circ C$]. Hereafter absolute humidity and relative humidity are called AH and RH, respectively, and AH3.1 represents an absolute humidity of 3.1 [g/m^3] and RH50 corresponds to relative humidity of 50[%].

2.3 10-degree-aperture cone model and yawed cylinder model

For free-stream noise evaluation in dry-air supersonic flow, the use of a total-pressure probe (identical to a Pitot tube) is preferable to a static-pressure measurement. This reason is based on the inherent nature that static-pressure fluctuations consist of contributions from both free-stream turbulence and fluctuations arising from boundary-layer physics which cannot, in general, be deconvolved. A total-pressure probe, however, is not always preferential for free-stream noise evaluation in the case of humid air as a working fluid. Because atmospheric humidity in the Muroran district varies considerably throughout the year, the evaluation of the free-stream disturbance environment must account for this seasonal variation. In an indraft tunnel drawing in atmospheric air, ambient water vapor changes into ice particles during the flow expansion through the nozzle, and downstream when these ice particles pass through the bow shock, they again change phase into water vapor or water droplets. If a Pitot tube were to be employed under such high humidity conditions, the stagnation point, where the pressure-sensing elements are placed, would be contaminated by water droplets. Consequently, the pressure sensor may indicate a misreading and perhaps more importantly, suffer from the possibility of deterioration or fatal damage due to water droplet impingement.

Boundary layers developing on the inside walls of the test section are turbulent under normal operation and static-pressure measurements on the inside walls of the test section are therefore unsuitable in the assessment of the free-stream static-pressure fluctuation, because turbulent motion in the boundary layer also spawns pressure fluctuations. To avoid this complication, static-pressure measurements for free-stream noise evaluation were conducted using an AEDC cone model rather than a Pitot-tube measurement.

In support of this, an AEDC 10-degree-aperture cone model was newly constructed for static-pressure measurements. A schematic of the cone model cross section is shown in Fig.3a, which indicates that the model has a total length of 250[mm] with a 70[mm] long stainless steel initial portion having a tip radius of 0.14[mm], and the remaining part of the cone made from the VESPEL® insulating material. The surface roughness of the metallic portion is approximately $0.21[\mu m]$ in the center-line averaged roughness, while the surface finish of the rest is, and the discontinuity between the metallic and VESPEL parts is less than $5[\mu m]$. A Kulite unsteady pressure sensor Model XCQ-62-350mBARD (5[PSI]=34.5[kPa]) with an external diameter of 1.65[mm] was vertically buried beneath a hole with a diameter of 0.5[mm] located 120 [mm] downstream of the tip. The distance between the cone surface and top surface of the pressure sensor should be as small as possible in order to avoid the influence of any Helmholtz resonance frequency. For the present model, the distance was fabricated at 0.5[mm], resulting in a resonance frequency of approximately 50[kHz], which is considerably higher than the rolloff frequency of 30[kHz]. Four static-pressure ports with a diameter 0.5mm spaced evenly at 90 degrees around the model 245[mm] downstream of the tip were installed with one port connected to the back pressure of the Kulite sensor. A Model CDV-700A DC amplifier manufactured by Kyowa Electronic Instruments was employed to condition the pressure signals.

Due to the concern of extremely low frequency components in the static pressure fluctuations raising the overall level, all waveforms were post-processed during data reduction to remove these components and their RMS values calculated in an Excel spreadsheet.

According to the existing database[12] regarding static-pressure fluctuations on the AEDC model, the transition Reynolds number is expected to be 5-6x10^6 under a mean-flow condition with a static-pressure fluctuation level of 0.1%-0.3% of the dynamic pressure. Therefore, the position of the installed pressure sensor was set to correspond to a Reynolds number of approximately 0.8 x10^6, to insure that boundary layer on the cone at that location retains the laminar state.

For 3-D boundary-layer transition studies, a stainless steel yawed circular cylinder model with a diameter of 40[mm] and a length of 500[mm] at a yaw angle of 60 degrees was fabricated. The model was installed in the test section in the vertical plane with both ends of the model cut so as to be parallel to the main stream. An oil-flow technique was employed to visualize the cylinder surface flow. The chemicals utilized for visualization were comprised of a mixture of oxide titanium, oleic acid and liquid paraffin mixed in the ratio of

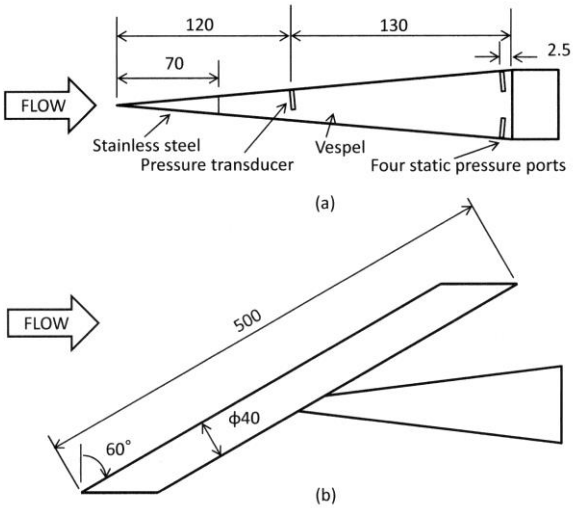

Fig. 3 Wind tunnel model. (a) 10-degree-aperture cone model, (b) yawed circular cylinder model. Unit in mm.

1:2:8. A video camera was employed to capture the cylinder surface oil flow under the Mach 2 flow condition, and a still camera was used at the end of the blow.

2.4 Data acquisition and analysis

All acquired analog data were stored in a data logger Model EZ-7510 supplied by NF Block, which has eight analog input ports with a resolution of 16 bits at the maximum sampling rate of 1MHz. For the present measurements, the sampling rate was set at either 100[kHz] or 200[kHz] per channel. An anti-aliasing filter (Nippon Audio Model PGF-8, 100dB/Oct) for each analog input port was used with the one-half frequency of the sampling rate. Acquired data from the unsteady pressure sensor and the photodiodes were reduced by the use of Matlab or Excel spreadsheet.

3 Experimental results

3.1 Evaluation of vapor condensation

As shown in Fig. 2, laser beams, which vertically permeate through the Schlieren window at the test section, are received by photodiodes on the other side of the test section, and the photodiode outputs in DC coupling mode are stored on the Logger EZ7510. Figure 4a compares four typical waveforms of the diode outputs acquired at various atmospheric conditions; i.e. (AH2.9, RH52), (AH5.0, RH44), (AH6.6, RH52) and (AH8.9, RH78). The vertical axis indicates the intensity of the received beam and is arbitrary but permits a relative amplitude comparison between wave -forms. Also, the waveforms are arbitrarily shifted on the horizontal time axis in this figure.

Prior to a given wind-tunnel blow, each waveform holds constant indicating no optical obstruction, but suddenly decreases at a certain time which corresponds to the starting time of the blow. Because the laser beam completely scattered initially, the photodiode output should be zero, showing that complete beam scatter in all cases is noticeable at the starting time. It is apparent that the light scatter is due to condensation of water vapors attendant in atmospheric air.

For the case of (AH6.6, RH52), small but regular periodic fluctuations superimposed on the photodiode output before and after the start time are observable and attributable to the hum component 100[Hz], because room lighting was turned on during the blow.

The four photodiode data plots shown in Fig.4 may be classified into two groups. For cases where AH is less than 6.6[g/m^3], it may be seen that photodiode output is held constant for an interval of 0.4 seconds right after the start, indicating that supersonic flow was steadily established. However, for the highest humidity case of AH8.9, a thick width of waveforms is observed, and the diode output oscillates periodically at 225[Hz] as shown in Fig.4b, where the time axis is enlarged. For this case, the mean intensity of the penetrated laser beam is reduced to 48% of that before the start and the peak to peak of its amplitude reaches as large as 65%. The origin of this large oscillation is related to the condensation process of water vapor present in the air near the supersonic throat. Also, it may be inferred that the high frequency selectivity of the oscillation is characteristic of a self-sustained oscillation.

For cases less than AH1.9, the photodiode output is observed to be virtually constant, except during the transient time right after the flow is started.

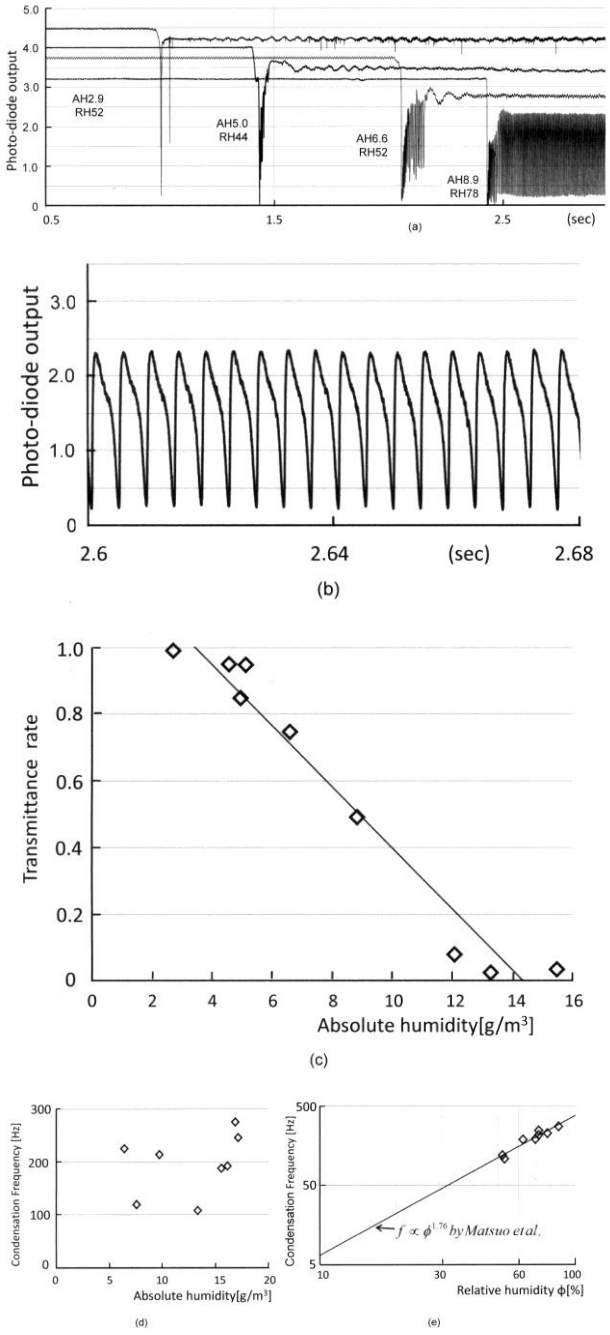

Fig. 4. Characteristic properties of permeated laser beam against humidity before and after the blow. (a) Comparison of photo-diode outputs, (b) Diode output in enlarged time scale in case of AH8.9, (c) Permeated beam ratio against absolute humidity, (d) Condensation-oscillation frequency against absolute humidity, (e) Condensation oscillation frequency against relative humidity.

Figure 4c shows a plot of the photodiode output against absolute humidity together with a straight line obtained from the least squares method. The intensity of the penetrated laser beam linearly increases as absolute humidity decreases. Figure 4c also shows that the beam

is completely intercepted by condensation in the case of absolute humidity larger than AH18, whereas for the case of absolute humidity less than AH2, no beam scatter at all was observed.

The periodic oscillation of condensation versus absolute humidity and relative humidity is illustrated in Fig.4d and 4e, respectively. The first appearance of periodic oscillation is observed for relative humidity larger than roughly 50% relative humidity as indicated by the waveforms shown in Fig.4a. Although periodic oscillation has no strong correlation with absolute humidity, it is expected that there is a certain relationship between oscillation frequency and relative humidity. To support this assertion, an empirical formula proposed by Matsuo et. al.[1] is also plotted in Fig.4e. This formula provides that the condensation frequency varies as relative humidity raised to the power of 1.76, times the total temperature T_0 to the power of 0.5, and exhibits good agreement with the present data assuming that T_0 is held invariable, due to the fact that the variation of T_0 is small in the present experiment.

In order to measure the convective velocity of the condensation fluctuation in the streamwise direction, five pairs of the laser-photo diodes spaced at an interval of 45mm and aligned in the flow direction, were simultaneously acquired as shown in Fig.5. In this figure, the photo diode output under the condition AH8.9 and RH78 (which is a case of the highest humidity in Fig.4a), is replotted for phase comparison. It should also be noted that the amplitudes of the five wave traces are evenly amplified, despite the fact that each photo-diode sensitivity to laser beam intensity is different. Nonetheless it is apparent that the phase of the diode outputs numbering from upstream to downstream, gradually decreases. The difference in phase between signals was calculated by means of the cross-correlation function.

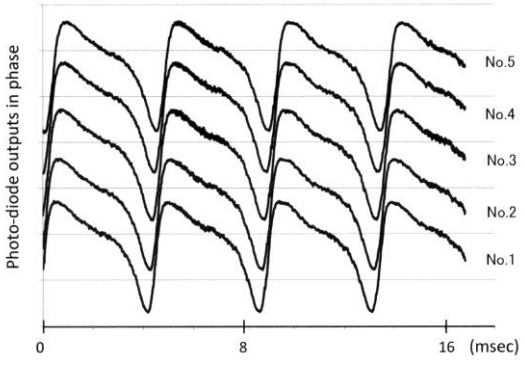

Fig. 5 Simultaneously acquired output traces of arrayed photo diodes.

As a result, the phase difference between the most upstream and the most downstream sensors is 0.356 [ms] for a spatial separation of 180[mm], corresponding to a phase velocity of 505[m/s], which is almost equal to the main stream velocity obtained from the Pitot-static measurement. Taking into account the accuracy of the Pitot static-tube measurement affected by humidity, it could be concluded that condensation fluctuation propagates downstream, convected by the main flow.

3.2 Static-fluctuation measurements on cone model

The previous results suggest that the oscillation of vapor condensation induces a static-pressure fluctuation in the test section and static-pressure fluctuation measurements using the 10-degree-aperture cone model are shown in Fig.6. Four typical time traces from static-pressure sensors under different humidity conditions are shown in Fig.6a and the corresponding spectrally analyzed results are shown in Fig.6b.

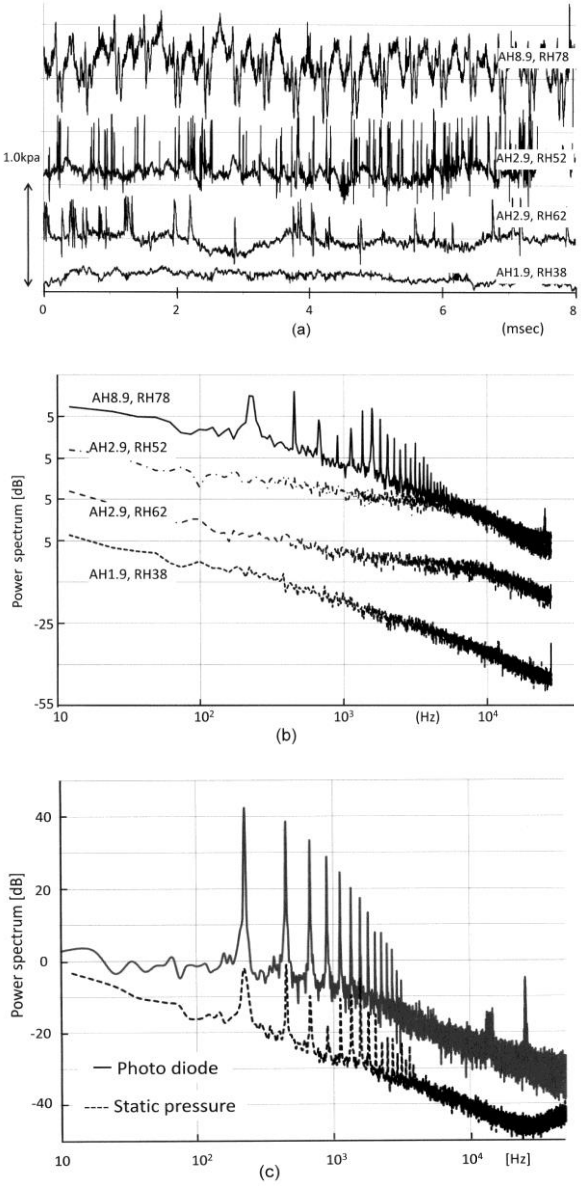

Fig. 6 Comparison of static-pressure fluctuation on cone model and photo-diode output against absolute humidity. (a) Waveforms of static-pressure fluctuations, (b) Power spectra of static-pressure fluctuations, (c) Power spectra of static-pressure fluctuation and photo-diode output.

Since the waveforms are shifted for comparison,

these amplitudes are comparable in each other. Also, corresponding power spectra also are shifted by +15 dB on the basis of the case of (AH1.9, RH38). A static pressure fluctuation for the case of the highest humidity (AH8.9, RH78) was previously illustrated in Fig.4 and is compared with the laser-photo diode measurements. It is expected that static-pressure fluctuation for the lowest humidity case (AH1.9, RH38) in terms of both absolute humidity and relative humidity, should be the smallest in amplitude. This result is consistent with the spectral analysis, indicating that there are no peculiar spectral components in the whole frequency range and spectral components tend to monotonically decrease as frequency is increased. For this case, the ratio of the intensity of the static-pressure fluctuation to the dynamic pressure is less than 0.1[%] as will be discussed later. On the other hand, for the case of the highest absolute humidity, the static pressure is observed to fluctuate periodically, and the peak to peak of the fluctuation reaches approximately 1[%] dynamic pressure. Also, spectral analysis of this fluctuation reveals discrete components corresponding to 225[Hz] and higher harmonics. The fact that this frequency agrees with that obtained from the laser-photo diode measurement suggests that the self-sustained oscillation due to condensation directly affects static pressure in the test section. For further confirmation, the spectrum of the photo-diode output is compared with that of static-pressure fluctuation in Fig.6c, where it is apparent that the periodic oscillations, including higher harmonic components are closely correlated with the AEDC cone measurements. Perhaps the most interesting point, however, is that except for these periodic oscillations, the baseline of the spectral components shows no difference between them, i.e. there are no irregular components present in the photo-diode output of Fig.5. This phenomenon is different from the other two cases of humidity level, without self-sustained oscillation due to condensation shown in Fig.4.

For the two cases of (AH2.9, RH52) and (AH2.9, RH62), which are the same absolute humidity, but different relative humidity, no clouded contamination was visibly perceivable and the laser intensity was reduced to -5[%] under (AH2.9, RH52), while for (AH2.9, RH62) no reduction in laser intensity occurs. The common phenomenon is spiky signals overriding on top of fluctuating static-pressure waveforms, indicating that spiky signals are more prevalent for lower relative humidity flow, rather than the higher case. As a consequence, a comparison of the spectra shown in Fig.6 shows that static-pressure fluctuation over the frequency range of 1-30 [kHz] is high compared with the other two cases as aforementioned. This suggests that such spiky signals not observed in the other two cases contribute to raising fluctuation components in the frequency range of 1-30[kHz]. The pulse width of the spiky signal is roughly 0.2[ms] to 0.5[ms] which corresponds to 120 to 240[mm] in the streamwise direction assuming that the flow velocity along the cone is roughly the same as that of the main flow (500[m/s]). The origin of fluctuations with this spatial scale may be inferred as follows: when tiny ice particles generated near the supersonic nozzle under high humidity conditions pass the conical shock wave at the tip of the cone model, a phase change from ice to liquid occurs, and the resulting liquid particles are retarded because of the endothermic latent heat process, which results in an increase of the static pressure. Therefore, it can be inferred that when phase changing particles pass near the pressure port, a positive pressure rise occurs. On the other hand, under the high humidity conditions which accompany self-sustained oscillation, the phase change of ice particles synchronizing with the oscillatory condensation, does not contribute to an increase of fluctuations in the 1-30[kHz] frequency range. In order to confirm the above speculation, simultaneous measurements of static pressure together with a hot-wire anemometer installed slightly downstream of the static pressure port are planned in the future. Also, in the case of (AH2.9, RH52), the output from the photo diodes sometimes indicates falling pulses, which may be ascribed to the passage of ice particles through the laser beam.

The RMS values of static-pressure fluctuation against absolute humidity and relative humidity are illustrated in Fig.7. The results show that as absolute humidity and/or relative humidity are decreased, pressure fluctuation level tends to decrease. It does not seem, however, that the level of static-pressure fluctuation is correlated with either absolute humidity or relative humidity. Nevertheless, Figure 7 shows that below AH2.0 a fluctuation level of 0.1% of the dynamic pressure of the flow obtains in the Muroran district in winter, which is generally regarded to be a quiet supersonic flow[13]. Under such low humidity atmospheric conditions as well as under the comparatively high humidity condition accompanying condensation oscillation, an experimental study regarding 3-D boundary-layer transition was conducted to document the effect of humidity on such a transition process.

3.3 Transition study on 3-D boundary layer

Surface-oil flow pattern on a yawed circular cylinder model is shown in Fig.8a for the case of (AH2.9, RH56). Although the flow quality did not satisfy the quiet supersonic flow condition with a static pressure fluctuation below 0.1[%] of dynamic pressure, Figure 8a is one of several captured snapshots, showing comparatively clear striations. The visualized region is downstream 30 degrees from the attachment line, because the flow near the critical point for the cross-flow instability is hypersensitive to surface roughness, resulting in triggering a row of stationary vortices. The 1mm scale and the azimuthal-angle scale ϕ from the attachment line are taken at the upper portion and at the right hand in the picture, respectively. Many striations downstream of $\phi = 40°$ are visible.

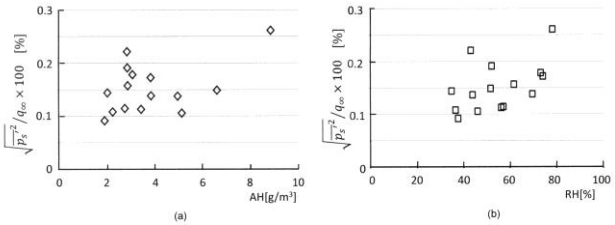

Fig. 7 Comparison of static-pressure fluctuation RMS, (a) Static-pressure fluctuation RMS against absolute humidity, (b) Static-pressure fluctuation RMS against relative humidity.

The wavelength λ along the white line parallel to the attachment line at $\phi = 50°$ was calculated by digital image analysis as shown in Fig.8b. This result shows

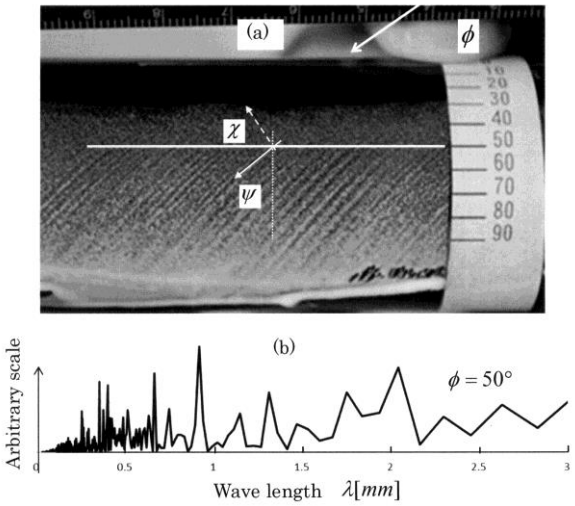

Fig. 8 Three-dimensional boundary layer transition on yawed cylinder model under (AH2.6, RH52), (a) Visualized pattern by surface-oil flow technique, (b) Spectrum by means of image analysis along white line at $\phi = 50°$ in Fig.8a.

approximately λ =0.9[mm], while compressible linear stability analysis[14] under the present experimental condition predicts this wavelength to be 0.82[mm]. Good agreement between experiment and analysis suggests that the striations may be attributable to the action of a row of stationary vortices originating from a cross-flow instability.

On the other hand, for the case of AH6.9 which is accompanied with the aforementioned self-sustained oscillation, video image visualized surface flow shows that although streaks were slightly visible at the incipient time of the blow, eventually the stationary structure disappeared by the end of the blow, as shown in Fig.9. It is suggestively shown that high free-stream disturbance flow is unfavorable for the growth of the stationary cross-flow mode.

Also, a traveling cross-flow mode under the extremely low humid environment was observed by means of hot-wire anemometer measurements and also compared with stability analysis. This time-dependent modes peaking at approximately 60kHz and growing downstream as shown in Fig.10a may be identified with the cross-flow instability mode[14].

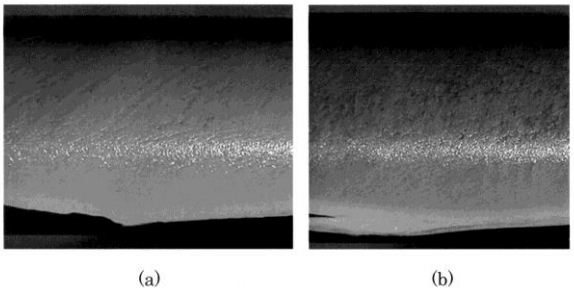

Fig. 9 Surface-oil flow pattern under absolute humidity of 6.9[g/cm³], (a) Flow pattern at two seconds after blow , (b) Flow pattern at six seconds after blow.

However, for the case of even slightly high humidity condition (AH2.12, RH60), similar hot-wire measurement at $\phi = 60°$ does not show the signature of the traveling mode, suggesting that the cross-flow instability is hypersensitive to free-stream turbulence. Under much higher humid condition (AH2.46, RH72), no distinct components are also observed as shown in Fig. 10b, in spite of growth of continuous components over wide range of frequency. Thus, since the influence of the free-stream noise level as well as the content of the free-stream noise is quite complex in the process of boundary-layer transition, further investigation is required.

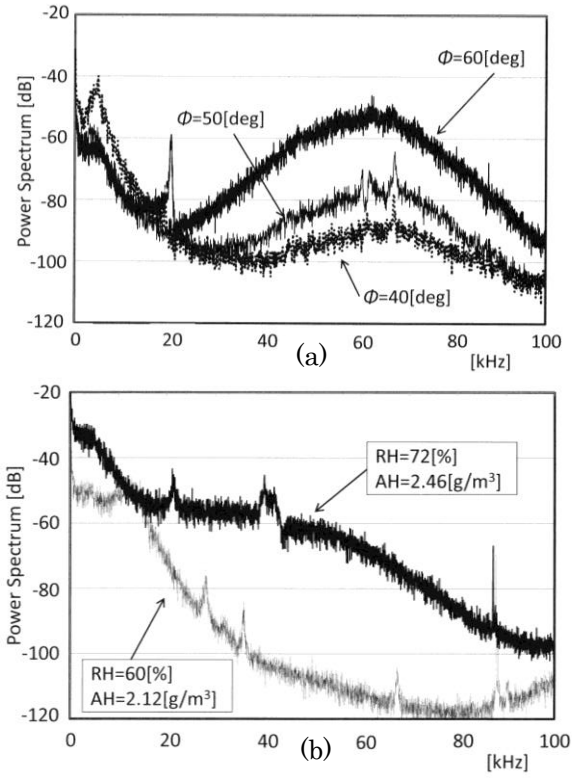

Fig.10 Power spectra of hot-wire anemometer output at various azimuthal position of the attachment line of yawed circular cylinder, (a) Power spectra of hot-wire anemometer output at various azimuthal positions and (b) Power spectra of hot-wire anemometer output at two different humid conditions.

4 Conclusion

The main flow of an indraft supersonic wind tunnel drawing air in from the ambient atmosphere is contaminated by the condensation of moisture present in the incoming air and the resulting flow properties are sensitive to atmospheric humidity. In order to quantitatively evaluate the influence of humidity at Mach 2 in the indraft supersonic wind tunnel located at the Muroran Institute of Technology, static-pressure fluctuations in the test section with the aid of a 10-degree-aperture cone model were measured. Also, moisture condensation was evaluated by the use of an array of laser-photo diodes beamed across the test section. Exploiting the characteristic feature that the cross-flow instability in 3-D boundary layers is hypersensitive to the flow properties, surface-oil flow visualizations and hot-wire measurements were employed to confirm the growth of stationary and traveling modes on the yawed circular cylinder. Several conclusions may be drawn from these investigations:

1) The ratio of the static-pressure fluctuation level to dynamic pressure is less than 0.1% when absolute humidity is below 2.0[g/m^3].
2) For absolute humidity in the range 2-6[g/m^3], positive pressure pulses overriding the static-pressure fluctuations increase over the frequency range of 1-30[kHz], with a spatial scale in the streamwise direction corresponding to 120-240[mm].
3) A train of positive pulses overriding the static-pressure fluctuation are ascribed to the passage of liquid particles accompanying latent heat release due to phase change from ice particles near the static -pressure port. Such static-pressure pulses are attributable to the endothermic process associated with the ice particles changing to liquid particles when they pass through the conical shock wave formed at the tip of the cone model.
4) Self-sustained oscillation due to liquid condensation occurs when an absolute humidity of 6[g/m^3] and relative humidity of 50[%] and [90%] exists in the ambient air.
5) Condensation oscillation results in increase of the static-pressure fluctuation in the test section.
6) Condensation oscillation advects with the main stream in the test section.
7) Under low absolute humidity conditions and the attendant low-turbulence environment, the stationary and traveling cross-flow modes on the yawed circular cylinder surface was observable, as predicted by compressible linear stability analysis.
8) For the case of slightly high humid environment compared with the previous case, growth of the traveling mode is suppressed, while free-stream turbulence flow with the accompanying self-sustained condensation oscillation, no stationary vortices appeared.

ACKNOWLEDGMENT

Compressible linear stability analysis associated with to the present experimental configuration was made by Professor S. Sakaue at Osaka Prefecture University. The authors would like to express their sincere appreciation. Also, thanks are extended to Mr. H. Ohtateme, graduate student, at Muroran Institute of Technology, who helped to conduct the present experiment and to reduce experimental data.

REFERENCES

(1) Matsuo, K., Kawagoe, S., Sonoda, K., and Setoguchi, T.: Flow oscillation in Laval nozzle accompanying condensation - part 1. Oscillatory range of occurrence and frequency, *J. of Jap. Soc. of Mech. Eng.* (B Series), **49** (1983), pp.108-114. (in Japanese)
(2) Matsuo, K., Kawagoe, S., Sonoda, K., and Setoguchi, T.: Flow oscillation in Laval nozzle accompanying condensation - part 2, Oscillatory amplitude and generation mechanism, *J. of Jap. Soc.of Mech. Eng.* (B Series), **50**(1984) pp.1319-1324. (in Japanese)
(3) Huang, J. C., Gault, R. I, Benard, E. and Raghunathan, S.: Effect of humidity on transonic flow, *J. Aircraft*, **45** (2008), pp. 2092-2099.
(4) Nagai, S., Tsuda, S., Koyama, T., Hirabayasi, N.: Humidity management for a hypersonic wind tunnel, *J. of Jap. Soc. for Aeronaut. Space Sci.*, **55** (2010), pp.483-489. (in Japanese)
(5) Herring, G. C.: Mach-number measurement with laser and pressure probes in humid supersonic flow, *AIAA J.*, **46** (2008), pp. 2107- 2108.
(6) Iriya, A., Yamamoto, S. and Daiguji, H.: Numerical method for transonic viscous flow considering humidity. *J. of Jap. Soc. of Mech. Eng.* (B Series), **62** (1996), pp.3854-3859. (in Japanese)
(7) Saric, S. W. and Reed, H. L.: *Ann. Rev. of Fluid Mech.*, **21** (1989), pp.235-284.
(8) Bippes, H.: Basic experiments on transition in three-dimensional boundary layers dominated by crossflow instability, *Progr. in Aerospace Sci.*, **35** (1999), pp.363-412.
(9) Takagi, S. and Itoh, N.: Observation of traveling waves in the three-dimensional boundary layer along a yawed cylinder, *Fluid Dyn.Res.*, **12** (1994), pp. 167-189.
(10) Minato. R, Mizobata, K., and Kuwada, K., Experimental Measurements of Starting Loads and Model Behaviors in the Indraft Supersonic Wind Tunnel, *Trans. of the Jap. Soc. for Aeronaut. Space Sci.,* **53.** (2010), pp.54-62.
(11) Daiichi Kagaku: Calculation of moisture : http://www.daiichi-kagaku.co.jp/situdo/notes/note108.html. (in Japanese)
(12) Dougherty, N. S., Jr.; and Fisher, D. F.: Boundary-Layer Transition on a 10-Deg Cone: Wind Tunnel/Flight Correlation. AIAA-80- 0154, 1980.
(13) Wolf, S.W.D., Laub, J.A. and King, L.S.: Flow characteristics of the NASA-Ames laminar flow super- sonic wind tunnel for Mach 1.6 operation, *AIAA* 94- 2502.
(14) Takagi, S., Sakaue, S., Hirata, Y., Uemura, T. and Takada, K.: Observation of Cross-Flow Instability Mode in a Yawed Cylinder Boundary Layer at Mach 2. *AIAA J.* **53**, No.1 (2015), pp.260-265